Carrier Dynamics in Quantum-Dot Multijunction Solar Cells Under Concentration

Alexandre W. Walker, Olivier Thériault, and Karin Hinzer

***Abstract*—The key performance metrics of quantum-dot (QD)-lattice-matched multijunction solar cells (MJSCs) composed of InGaP/(In)GaAs/Ge with InAs/GaAs QDs are explored under high-concentration illumination with a focus on the carrier dynamics in the QD layers of the middle subcell. An effective medium approach is used to describe generation and recombination in the QD system, including carrier escape and capture from the weakly confining quantum well and the QD states. At a concentration of 1000 suns, simulations indicate that the specific QD MJSC studied outperforms a standard MJSC by 1.1% in relative efficiency operating at 25 °C. However, this gain in efficiency is highly dependent on the confinement potentials of the wetting layer, as well as the resulting current mismatch between the top and middle subcells when carrier escape rates from within the wetting layer confinements are reduced.**

***Index Terms*—Carrier dynamics, concentrator photovoltaics, multijunction solar cells (MJSCs), quantum dots (QDs), III–V semiconductors.**

I. Introduction

THE current research avenue in developing next-generation photovoltaic devices with efficiencies reaching 50% is aligned toward concentrated photovoltaics to focus sunlight onto smaller device areas. This allows for a reduction in the growth and manufacturing costs associated with III–V multijunction solar cells (MJSCs), and also increases device efficiency due to the effects of concentration. The current state-of-the-art triple-junction solar cells, such as the lattice matched device composed of $In_{0.49}Ga_{0.51}P/In_{0.01}Ga_{0.99}As/Ge$, are currently capable of achieving greater than 40% efficiency at concentrations of ~400 suns [1]. However, this MJSC design does not exploit the ideal combination of bandgaps, since the Ge subcell overproduces photocurrent by as much as 60% compared with the top two subcells. The excess photocurrent is dissipated as heat, which results in some performance degradation.

An alternative design to this device architecture is obtained by exploiting the self-assembled growth of low-dimensional semiconductor heterostructures such as InAs quantum dots (QDs) on an InAs wetting layer (WL) within the InGaAs subcell. The zero-dimensional confinement effects in these nanostructures have been shown to produce controlled and reproducible energy transitions [2] with strong wave function overlap [3]. As a result, these nanostructures can be size engineered to harness photon energies below the bandgap of the bulk material, which leads to a redistribution of current from the bottom Ge subcell to the middle subcell [4], [5]. Combined with an optimized top subcell bandgap using sublattice ordering effects in InGaP [6], the short-circuit current density (J_{sc}) of the full device can be increased under 1-sun illumination [4], [7]. This strategy can potentially be exploited to increase the overall device efficiency depending on the drop in the open-circuit voltage (V_{oc}) and fill factor (*FF*) arising from introducing lower bandgap structures in the middle subcell. Achieving near 1-V open-circuit voltage for a single-junction GaAs solar cell containing InAs/GaAs QD has been recently shown in the literature [8] and is a very promising feat for MJSC applications. In order to achieve an overall boost in the performance, however, the carrier dynamics near these low-dimensional semiconductor heterostructures must be understood in greater detail since these affect recombination rates that inherently dictate the V_{oc} and *FF*, and therefore, the overall efficiency (η). Additionally, these effects must also be studied over concentration where the competition between radiative and nonradiative recombination rates impacts the cell's overall performance.

In this paper, we present a study on the effects of carrier dynamics in the InAs/InGaAs QD system on the overall performance of an InGaP/InGaAs/Ge MJSC. This study builds on our previous work in developing a numerical model of a QD MJSC, which focused on the generation and recombination in the QD layers [4]. We first give a brief outline of the model before discussing how the carrier dynamics are treated in the numerical modeling environment. This model is created using version vG-2012.06 of TCAD Sentaurus by Synopsys, where the transport equations are handled by Sentaurus Device's finite difference and finite-element methods. The performance of the QD MJSC is then simulated under standard testing conditions (1 kW/m^2, AM1.5D spectrum at 300 K) before the performance over concentrated illumination is explored.

II. Structure and Model

The MJSC structure consists of a dual-layered antireflection coating composed of Si_3N_4 and SiO_2, a top InGaP subcell connected in series to an InGaAs subcell via an AlGaAs/GaAs tunnel junction, which is also connected in series to a Ge bottom subcell via a similar TJ. The top contact has a 10-mΩ series resistance. Within the intrinsic region of the middle InGaAs *n-i-p* subcell are 110 layers of an effective medium describing the InAs QD and the associated WL. This configuration was determined to be near optimal in terms of efficiency as a function of the number of QD layers [9]. The effective medium has

Manuscript received July 5, 2013; revised April 9, 2014; accepted April 29, 2014. Date of publication June 6, 2014; date of current version June 18, 2014. This work was supported in part by NSERC, OGS, MRI, CFI, and Canada Research Chair.

A. W. Walker was with the Department of Physics, University of Ottawa, Ottawa, ON K1N 6N5, Canada. He is now with Fraunhofer ISE, 79110, Freiburg, Germany (e-mail: awalk102@uottawa.ca).

O. Thériault and K. Hinzer are with the Department of Physics, University of Ottawa, Ottawa, ON K1N 6N5, Canada (e-mail: other005@uottawa.ca; khinzer@uottawa.ca).

Digital Object Identifier 10.1109/JPHOTOV.2014.2322279

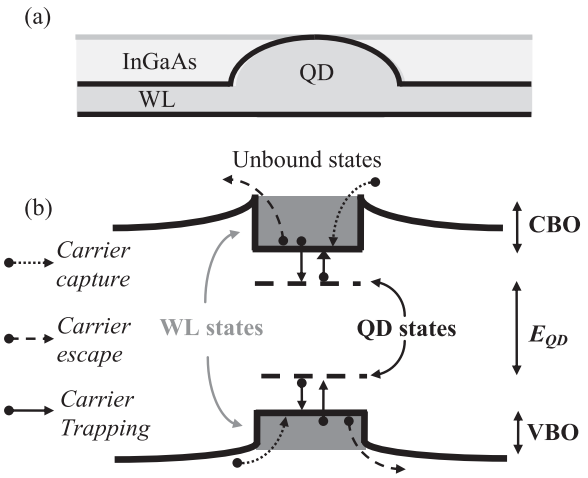

Fig. 1. (a) Geometry of the InAs WL and QD with part of the InGaAs spacer layer; this forms the effective medium. (b) Carrier dynamics between bound and unbound states in the InAs/InGaAs QD system, where carrier escape and capture are modeled using thermionic emission into and out of the bound states. E_{QD} is the ground state transition energy of the QD, and both QD ground states are modeled as shallow trap states. CBO and VBO are the conduction and valence bands, respectively.

a total thickness of 1.7 nm [see Fig. 1(a)], and adjacent QD layers are separated by 8.3 nm of intrinsic InGaAs spacer layers such that tunneling between adjacent layers is not significant; a repeat layer is, therefore, 10 nm thick. The middle subcell base thickness is reduced in the QD MJSC to maintain a total subcell thickness of 4 μm for comparison with the control structure. It is assumed the rapid thermal annealing and indium flush techniques allow for the growth of a high number of layers with pristine material quality [10]. Such strain management avoids the requirement for strain compensation layers such as GaAsP, which would increase the potential barrier relevant for carrier escape out of the QDs. However, more studies would be required to assess the impact of such layers on the carrier dynamics. For details on the numerical modeling environment, the structure including tunnel junctions, and the QD effective medium, see [4], [5], [9], [11], and [12].

Fig. 1(a) shows the geometry of nanometer-sized islands of InAs QDs on top of the thin WL grown by the Stranski–Krastanov growth method [13], and Fig. 1(b) illustrates a schematic representation of the energy band alignment in this system, which is explained below. The single confined electron energy level expected from the dimension of these dots corresponds to a single ground-state energy transition centered at 920 nm [see the external quantum efficiency (EQE) illustrated in Fig. 2(a)]. The lens-shaped QDs are modeled based on a distribution of sizes with average radii and heights of $\bar{r} = 5.6$ nm and $\bar{h} = 0.6$ nm, respectively, and the WL has a thickness of 1.1 nm. The absorption coefficient of these nanostructures is calculated using energy levels obtained by numerically solving Schrodinger's equation based on the given QD and WL geometry [4]. A Gaussian distribution in energy levels is implemented. The modeled QD density is 125 QD/μm^2, which is comparable with typical values in the literature [13]. The QD hole and electron ground-state energy levels are modeled as trap levels above and below the valence and conduction bands, respectively, according to a Gaussian distribution in energy with the same full-width at half maximum as the absorption coefficient calculation. Although multiple hole levels exist due to its larger effective mass, it is assumed that holes quickly relax to the ground state such that only this level is pertinent to recombination processes. Furthermore, only the ground-state energy transition contributes to the absorption coefficient since the overlap integral decreases strongly for $n \neq m$ transitions [3]. The trap levels add to the bulk Shockley–Read–Hall (SRH) recombination rates in the effective medium based on a trap cross section of 10^{-13} cm^{-2} (according to the QD geometry) and a trap concentration corresponding to the QD density per layer. The effective medium also considers minority carrier lifetimes for radiative (1 ns) and nonradiative (10 ns) recombination processes and weighted based on volume considerations within the effective medium [4].

Carriers photogenerated in the bound states of the nanostructures must first escape into the unbound states to contribute to the bulk current of the device, as illustrated in Fig. 1(b). The dominant process for this escape is carrier-optical phonon scattering at room temperature [14]. The opposite process, i.e., carrier capture from the bulk states to the WL and subsequently to the QD states, must also be treated. These carrier capture processes are known to occur on picoseconds time scales [14], [15]. A separate quasi-Fermi level for the bound states is required to properly describe the exchange between bound and unbound carrier populations for the WL. Doing so results in a supplementary set of continuity equations for minority carriers [16]. However, implementing these supplementary equations in Sentaurus Device leads to an overestimation of the generation since no generation rates are considered in the continuity equation dictating bound carrier concentrations; in other words, generation is assumed only for the unbound carrier populations.

Consequently, an effective band offset approach is adopted. Thermionic emission is used to model the escape of carriers from the WL to the unbound states, which is parameterized by the height of the potential barrier. This method uses the electron affinity and bandgap of the effective medium to control the conduction and valence band offsets (CBO and VBO, respectively) with respect to the spacer InGaAs layer [see Fig. 1(b)]. An assumption of the model is that all photogenerated carriers are captured by the WL. The carriers confined to the WL can be captured by available trap states modeling the energy levels of the QD [carrier trapping in Fig. 1(b)], or escape from the potential confinement of the WL. Different levels of band offsets mimic different escape rates from the WL. It is important to note that band offsets totaling 7 meV represents the simulated energy difference between the bulk InGaAs bandgap and the WL ground state based on COMSOL Multiphysics simulations of the energy levels [4].

III. Simulation Results

A. One-Sun Conditions

Fig. 2 illustrates the simulated room temperature (a) EQE and (b) current–voltage (J–V) characteristics of the device for various scenarios of band offsets assuming uniform illumination according to the AM1.5D spectrum at 300 K [illustrated as

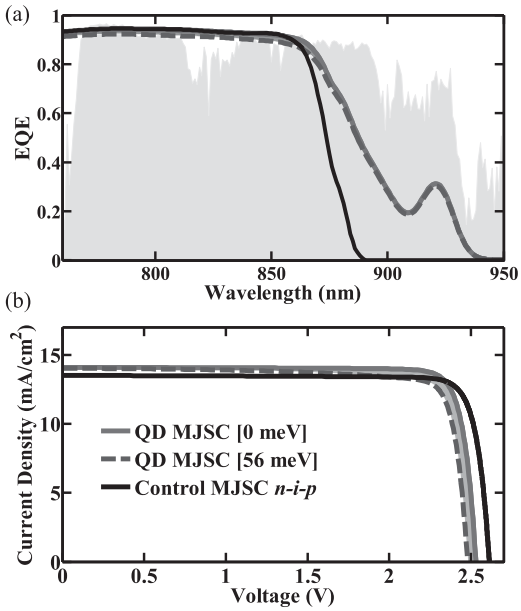

Fig. 2. (a) Simulated EQE at room temperature of a QD enhanced MJSC within the range of the middle InGaAs subcell for different combinations of CBO and VBO between 0 and 56 meV (dark gray area represents the range in between the band offsets). The normalized AM1.5D solar spectrum is shown in grey in the background. (b) Simulated current–voltage characteristics at 1-sun (1 kW/m^2) compared with the control structure with an *n-i-p* middle subcell configuration.

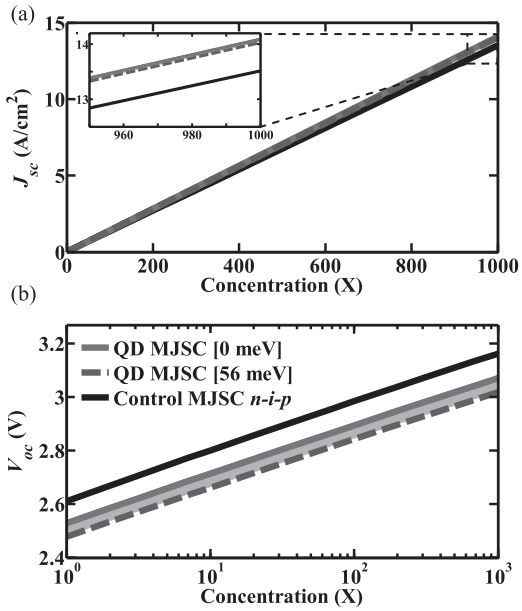

Fig. 3. Simulated (a) $J_{\rm sc}$ and (b) $V_{\rm oc}$ as a function of concentration for 0 and 56 meV of effective band offsets (and scenarios in between); the simulated data is compared with a control structure with an *n-i-p* middle subcell configuration without QDs.

a normalized photon flux in light gray in Fig. 2(a)]. Fig. 2(a) illustrates the enhanced quantum efficiency of the middle subcell to photon energies below the bandgap of bulk InGaAs, and thus a redistribution of current from the overproducing bottom Ge subcell to the middle subcell. This is manifested as an overall higher photocurrent than a control MJSC with no QDs, which is illustrated in Fig. 2(b). Ideally, carriers are not captured by the WL states, and all carriers escape, which is modeled as 0 meV of band offsets; this scenario still adopts the weighted minority carrier lifetimes corresponding to the nanostructures and, therefore, decouples the effects of lower bandgap and increased recombination rates due to carrier capture. The EQE and *J–V* characteristics for the 0 meV band offset scenario have the highest $J_{\rm sc}$, $V_{\rm oc}$, *FF*, and η. The worst-case scenario, on the other hand, involves effective band offsets that reach the ground-state QD energy levels at 920 nm (42 meV below the conduction band and 14 meV above the valence band). The range of band offsets between the 0-meV best case scenario and the 56-meV worst-case scenario is explored and illustrated as a gray band in terms of the EQE and *J–V* characteristics in Fig. 2(a) and (b). As the effective band offsets are increased, the response of the cell to wavelengths between 700 and 890 nm decreases due to the reduced escape rates for carriers captured by the QD effective medium. On the other hand, the response for wavelengths targeted by the nanostructures (890–920 nm) is not affected as significantly by these band offsets. This originates from the fact that carriers generated in the confinement potentials readily escape at room temperature, even for the largest band offsets considered. Consequently, a minor decrease in photocurrent is expected as a function of increasing band offsets, which is apparent in Fig. 2(b). However, the most important effects of increasing the band offsets are manifested in the *FF* and $V_{\rm oc}$. As band offsets are increased, carriers are less likely to escape from the confinement potentials of the WL, which becomes important at higher voltages due to the exponential dependence of the recombination rates on voltage. Interestingly, the *FF* decreases more than the $V_{\rm oc}$ since the device ceases to be perfectly current matched (CM) for higher band offsets: the middle subcell has a $J_{\rm sc}$ lower than the top subcell $J_{\rm sc}$ by $\sim$1% absolute. The effects of current mismatch become clearer when studying the trends over concentration, which are discussed in the next section. A comparison between CM and current mismatched (CMM) cells is also given.

B. Concentrated Illumination Conditions

Simulations conducted over concentration (X) at constant temperature (300 K) are presented in Fig. 3 in terms of (a) $J_{\rm sc}$ and (b) $V_{\rm oc}$. The photocurrent illustrates the expected linear relationship as a function of concentration with no photon recycling effects. All of the effective band offset scenarios show a similar photocurrent increase [see the inset of Fig. 3(a)]. The control MJSC photocurrent is lower than the 0-meV QD MJSC by 4.3% throughout the entire range of concentration. It is worth noting that the saturation of the energy levels in the QDs is expected to appear at extremely high concentration [17]. This is why the QD MJSC is in the linear regime, with the absorption coefficient staying constant for increasing light intensities. Fig. 3(b) illustrates that $V_{\rm oc}$ increases logarithmically with concentration for all cases. The absolute drop in $V_{\rm oc}$ for the QD MJSC relative to the control is similar at 1 and 1000 suns. The 0-meV band offset scenario demonstrates a voltage drop that arises due to the lower minority carrier lifetimes of the effective medium compared with bulk InGaAs. It becomes clear that increasing the magnitude of the band offsets results in an increased drop in $V_{\rm oc}$ due to the decreased escape rates from the deeper WL

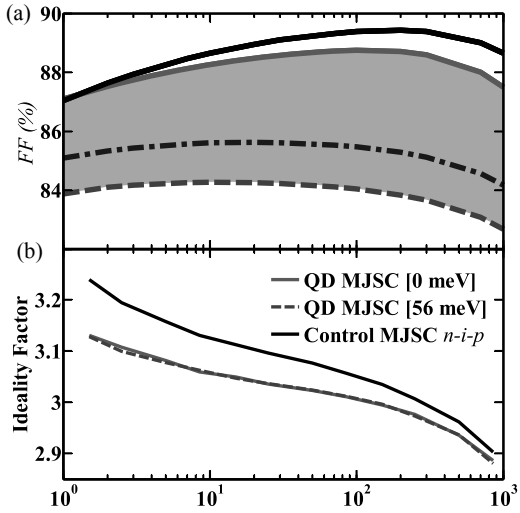

Fig. 4. Simulated (a) *FF* and (b) ideality factor as a function of concentration for 0 to 56 meV of effective band offsets. The simulated data is compared to a control structure with an *n-i-p* middle sub-cell configuration without QDs. The ideality factor was extracted using the slope of the open circuit voltage over concentration based on equation (1).

potentials. The escape rates are thus intricately connected to the middle subcell's dark current: decreased escape rates increase the overall recombination rates via added recombination terms in the supplementary continuity equations [4].

Fig. 4 illustrates (a) *FF* and (b) the ideality factor as a function of concentration. The trends in the *FF* reveal a few particular artefacts of this specific MJSC design, such as series resistance and current matching effects. First, the *FF* of the control increases logarithmically over concentration up to 200 suns and then starts decreasing due to the 10-mΩ series resistance of the top contact. The *FF* of the QD MJSC structures demonstrates a similar roll-off. Second, increased band offsets have a significant impact on the *FF* due to the change in current matching between the top and middle subcells. For band offsets below 20 meV, the top and middle subcells are adequately CM (within 0.3%). However, as the band offsets increase beyond 20 meV, the middle subcell begins to limit the overall photocurrent of the device, which is manifested primarily as a drop in the *FF*. This partly explains the $\sim$4% absolute drop between the best-case 0-meV and worst-case 56-meV scenarios. The decreasing $V_{\rm oc}$ as a function of increasing band offsets also contributes to the drop in *FF*. Current matching the device specifically for this worst-case scenario enhances the *FF* by 1.5% absolute at 1000 suns, and this is illustrated in Fig. 4(a) for a CM MJSC compared with a CMM device. These structures differ simply by the top subcell base thickness, and both have very similar $J_{\rm sc}$ and $V_{\rm oc}$ metrics. Another interesting trend is the split in the *FF* between the 0-meV QD MJSC and the control beyond 1 sun. This split arises from the larger increase in $V_{\rm oc}$ over concentration of the control MJSC, which is illustrated by the larger ideality factor of the control compared with the QD MJSC in Fig. 4(b). The ideality factor was obtained from the slope of $V_{\rm oc}$ over concentration based on

$$V_{\rm oc} = \frac{nkT}{q}\log\left(X\right) + V_{\rm oc}\left(X=1\right). \qquad (1)$$

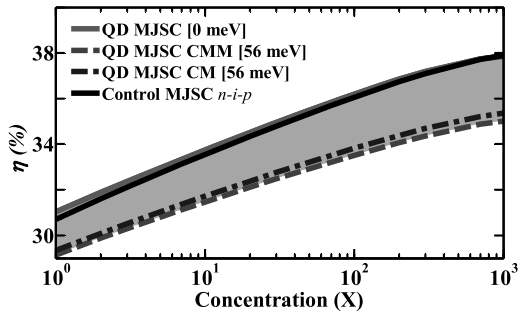

Fig. 5. Simulated efficiency η as a function of concentration X. The simulated data is compared to a control structure with an *n-i-p* middle sub-cell configuration without QDs.

The ideality factors from Fig. 4(b) are in agreement with those obtained for similar structures [18]. The control's larger ideality factor originates primarily from the strong SRH recombination taking place in the depletion region of the control's middle subcell, whereas radiative recombination dominates the depletion region in the QD MJSC at $V_{\rm oc}$. Although the increase in $V_{\rm oc}$ over concentration appears identical for each structure [see Fig. 3(b)], the control has an ideality factor closer to $n = 3.3$ at 1 sun, as compared with the QD MJSC which is closer to $n = 3.15$. This demonstrates the impact of the ideality factor on the *FF* over concentration. The difference in the ideality factor for all devices becomes negligible at higher concentration, since the *FF* becomes dominated by series resistance, which is the same in each device studied.

Finally, the QD MJSC as a function of concentration is illustrated in Fig. 5. The efficiency of the QD MJSC with 0 meV of band offsets is higher than the control over all concentrations explored. As mentioned before, the roll-off in efficiency observed at higher concentrations is due to the series resistance of the structure. An overall efficiency of 31% at 1 sun is observed for the 0-meV band offset scenario, which is a relative boost in efficiency of 1.1% over the control. For band offsets greater than $\sim$10 meV, however, the efficiency decreases beyond that of the control structure. This trend is once again predominantly due to the decreased *FF* arising from the current mismatch. With a perfectly CM device for the worst-case scenario, the efficiency improves from 35% to 35.4%, as illustrated in Fig. 5. The results of Figs. 3 and 4 thus outline the importance of the added recombination mechanisms arising from the escape of carriers from the confinement potentials of the WL on QD MJSC efficiency over concentration. The performance benefits arising from the increased photocurrent of a QD MJSC depend intricately on the confinement properties of the WL in terms of the escape rates and their effects on the current matching between the top and middle subcells. In general, QD MJSC device designs can be further improved by optimizing the number of QD layers, the background doping of the intrinsic region in the middle subcell, and the size and geometry of the dots. The effects of realistic operating temperature for cells illuminated under 1000 suns (60–80 °C) could potentially reduce the impact of the WL band offsets on performance by increasing the escape rates. This offers a potential enhancement factor over a control MJSC, although this hypothesis merits further study.

IV. Conclusion

In conclusion, the performance of an MJSC enhanced with low-dimensional semiconductor heterostructures, such as the InAs/GaAs QD system, has been explored as a function of concentration. A relative increase of 1.1% efficiency is achievable over a control MJSC structure at 1-sun intensity, assuming no confinement potentials in the WL. At 1000 suns, the efficiencies are nearly identical, although realistic operating temperatures are expected to give the QD MJSC an advantage over a control MJSC by enhancing the escape rates of carriers from the WL and QDs. The enhanced middle subcell response to photon energies below the bandgap of bulk InGaAs thus provides a method of bandgap engineering a MJSC to provide higher overall device photocurrent. This allows MJSC designs more control of the cell's responsivity to specific spectral conditions that depend on geographic location and on effects arising from the concentrator optical transfer function.

Acknowledgment

The authors would like to thank CMC Microsystems, for the licensing of TCAD Sentaurus, and Cyrium Technologies, Inc., for providing their first-generation QDEC samples for testing and characterization.

References

[1] R. R. King, A. Boca, W. Hong, X.-Q. Liu, D. Bhusari, D. Larrabee, K. M. Edmondson, D. C. Law, C. M. Fetzer, S. Mesropian, and N. H. Karam, "Bandgap engineered architectures for high-efficiency multijunction concentrator solar cells," presented at the 24th Eur. Photovoltaic Solar Energy Conf. Exhib., Hamburg, Germany, Sep. 21–25, 2009.

[2] B. J. Riel, "An introduction to self-assembled quantum dots," *Amer. J. Phys.*, vol. 76, no. 8, pp. 750–757, 2008.

[3] V. Popescu, G. Bester, and A. Zunger, "Coexistence and coupling of zero-dimensional, two-dimensional, and continuum resonances in nanostructures," *Phys. Rev. B*, vol. 80, pp. 045327-1–045327-12, 2009

[4] A. W. Walker, O. Thériault, J. F. Wheeldon, and K. Hinzer, "The effects of absorption and recombination in quantum dot multi-junction solar cell device efficiency," *J. Photovoltaics*, vol. 3, no. 3, pp. 1118–1124, May 2013.

[5] A. W. Walker, J. F. Wheeldon, O. Thériault, M. Yandt, and K. Hinzer, "Temperature dependent external quantum efficiency simulations and experimental measurement of lattice matched quantum dot enhanced multijunction solar cells," in *Proc. 37th IEEE Photovoltaic Spec. Conf.*, Seattle, WA, USA, Jun. 2011, pp. 000564–000569.

[6] A. Luque and S. Hegedus, *Handbook of Photovoltaic Science and Engineering*. New York, NY, USA: Wiley, 2003, Ch 9.6.3.2, p. 387.

[7] C. Kerestes, S. Polly, D. Forbes, C. Bailey, S. M. Hubbard, J. Spann, P. Patel, and P. Sharps, "Investigation of quantum dot enhanced triple junction solar cells," in *Proc. 37th IEEE Photovoltaic Spec. Conf.*, Seattle, WA, USA, Jun. 2011, pp. 19–24.

[8] C. Bailey, D. V. Forbes, R. P. Raffaelle, and S. M. Hubbard, "Near 1 V open circuit voltage InAs/GaAs quantum dot solar cells," *Appl. Phys. Lett.*, vol. 98, pp. 163105-1–163105-3, 2011.

[9] A. W. Walker, O. Theriault, and K. Hinzer, "The dependence of multijunction solar cell performance on the number of quantum dot layers," *IEEE J. Quantum Electron.*, vol. 50, no. 3, pp. 198–203, Mar. 2014.

[10] H. C. Liu, M. Gao, J. McCaffrey, Z. R. Wasilewski, and S. Fafard, "Quantum dot infrared photodetectors," *Appl. Phys. Lett.*, vol. 78, no. 1, p. 79, 2001.

[11] J. F. Wheeldon, A. Walker, C. E. Valdivia, S. Chow, O. Thériault, R. Beal, M. Yandt, F. Proulx, D. Masson, B. Riel, D. McMeekin, N. Puetz, S. G. Wallance, V. Aimez, R. Ares, T. J. Hall, S. Fafard, and K. Hinzer, "Efficiency measurements and simulations of GaInP/InGaAs/Ge quantum dot solar cells at up to 1000-suns under flash and continuous concentration," in *Proc. AIP Conf.*, 2011, vol. 1407, pp. 220–223.

[12] A. W. Walker, O. Thériault, M. Wilkins, J. F. Wheeldon, and K. Hinzer, "Tunnel-junction-limited multijunction solar cell performance over concentration," *IEEE J. Sel. Topics Quantum Electron.*, vol. 19, no. 5, art. no. 4000508, Sep./Oct. 2013.

[13] S. Fafard, Z. R. Wasilewski, C. Ni. Allen, D. Picard, M. Spanner, J. P. McCaffrey, and P. G. Piva, "Manipulating the energy levels of semiconductor quantum dots," *Phys. Rev. B*, vol. 59, no. 23, p. 15368, 1999.

[14] M. De Giorgi, C. Lingk, G. Von Plessen, J. Feldmann, S. De Rinaldis, A. Passaseo, M. De. Vittorio, R. Cingolani, M. Lomascolo, "Capture and thermal re-emission of carriers in long-wavelength InGaAs/GaAs quantum dots," *Appl. Phys. Lett.*, vol. 79, p. 3968, 2001.

[15] G. A. Narvaez, G. Bester, and Alex Zunger, "Carrier relaxation mechanisms in self-assembled (In,Ga)As/GaAs quantum dots: Efficient P to S Auger relaxation of electrons," *Phys. Rev. B*, vol. 74, p. 075403, 2006.

[16] S. M. Ramey and R. Khoie, "Modeling of multiple-quantum-well solar cells including capture, escape and recombination of photoexcited carriers in quantum wells," *J. Quantum Electron.*, vol. 50, no. 5, pp. 1179–1188, 2003.

[17] O. Thériault, A. W. Walker, J. F. Wheeldon, and K. Hinzer, "Effects of quantum dot layers on the behaviour of multi-junction solar cell operation under concentration," in *Proc. AIP Conf.*, 2012, vol. 1477, pp. 20–23.

[18] G. S. Kinsey, P. Hebert, K. E. Barbour, D. D. Krut, H. L. Cotal, and R. A. Sherif, "Concentrator multijunction solar cell characteristics under variable intensity and temperature," *Prog. Photovoltaics, Res. Appl.*, vol. 16, pp. 503–508, 2008.

Alexandre W. Walker received the B.Sc. degree in astrophysics from Queen's University, Kingston, ON, Canada, in 2007 and the M.Sc. and Ph.D. degrees in physics from the University of Ottawa, Ottawa, ON, in 2008 and 2013, respectively.

During his M.Sc. research, he was with UBM TechInsights in conjunction with the University of Ottawa. Following this, he was a member of the University of Ottawa's Sunlab from 2009 until 2013 for his doctorate studies. He then moved to Fraunhofer ISE in Freiburg, Germany, for postdoctoral research in 2013. His research interests include modeling and simulation of high efficiency III-V photovoltaic devices for next-generation concepts. Overall, he has contributed over 30 publications and conference proceedings in the field. He has been a member of the Photovoltaic Innovation Network since 2010.

Olivier Thériault received the B.Sc. degree in physics from the Université de Sherbrooke, Sherbrooke, QC, Canada, in 2009. He is currently working toward the Ph.D. degree in physics with the University of Ottawa, Ottawa, ON, Canada.

His research interests include the implementation of nanostructures, such as quantum dots in third-generation solar cells. He is in charge of the experimental characterization of these structures and plays an important role in modeling them.

Mr. Thériault received a Natural Sciences and Engineering Research Council PGS-D Scholarship in 2010.

Karin Hinzer received the B.Sc., M.Sc., and Ph.D. degrees in physics from the University of Ottawa, Ottawa, ON, Canada, in 1996, 1998, and 2002, respectively.

She is currently an Associate Professor and Canada Research Chair in Photonic Nanostructures and Integrated Devices and an Associate Professor with the School of Electrical Engineering and Computer Science, University of Ottawa. She has made pioneering contributions to the experimental physics of quantum dots marked by two landmark papers in *Science*. She gained extensive experience in the design and fabrication of group III–V semiconductor devices while with the National Research Council Canada, Nortel Networks, and Bookham. Cost-reduction strategies and liaison with remote fabrication facilities strongly feature in her industry experience. She joined the University of Ottawa in 2007, where she is the Founder of the SUNLAB, which is a modeling and characterization laboratory specializing in the development of high-efficiency solar cells. Since the laboratory's inception, she has trained more than 40 highly qualified personnel in the field of photovoltaic material and devices. Since 2010, she has been with the inorganic photovoltaics Cotheme Leader within the Pan-Canadian Photovoltaic Research Network.

Dr. Hinzer received the Inaugural Canadian Energy Award, with industry partner Morgan Solar, for the development of more efficient solar panels, in 2010.